Journal of Electroceramics 4:S1, 69–80, 1999

Valence Band Structure of ZnO $(10\bar{1}0)$ Surface by Cluster Calculation

KATSUYUKI MATSUNAGA*, FUMIYASU OBA, ISAO TANAKA & HIROHIKO ADACHI
Department of Materials Science and Engineering, Kyoto University Sakyo-ku, Yoshida, Kyoto, Japan, 606-01

Submitted November 14, 1997; Revised May 21, 1998; Accepted June 12, 1998

Abstract. Discrete variational (DV) $X\alpha$ cluster method has been employed in calculating electronic structures of ZnO. Electronic structures of the bulk and the non-polar surface model clusters are calculated with inclusion of electrostatic potentials in the bulk and near the surface, and the electronic origins of experimental spectra and chemical bonds at the surface are examined in detail. The valence band structure constructed by Zn-3*d* and O-2*p* bands is much influenced by electrostatic potentials in ZnO. It is found that the reduction of an electrostatic potential near the surface gives rise to the difference of the valence band structures between in the bulk and at the surface. The calculated density of states at the non-polar surface of ZnO, where the Zn-3*d* and O-2*p* bands are more widely separated than in the bulk, is in good agreement with the experimental UPS. In addition, a Zn-O bond at the surface is found to show stronger covalency than that in the bulk, as a result of the change of the valence band structure due to the effect of the electrostatic potential.

Keywords: molecular orbital, DV-$X\alpha$ method, non-polar surface, valence band

1. Introduction

Zinc oxide (ZnO) is one of a class of important functional ceramics widely used as a catalyst, a gas sensor and a varistor. These distinctive phenomena of ZnO are thought to originate from electronic properties in the vicinity of its surfaces or grain boundaries [1,2]. For the purpose of interpreting these phenomena, understanding of the electronic structure of the ZnO surface is essential.

The non-polar $(10\bar{1}0)$ surface of ZnO is known to be a cleavage face and a catalytically active surface [1,3]. Experimental UPS (ultraviolet photoelectron spectroscopy) and XPS (X-ray photoelectron spectroscopy) measurements [3–9] have revealed that the valence band of the ZnO $(10\bar{1}0)$ surface is composed of Zn-3*d* and O-2*p* orbitals, and that the Zn-3*d* band is not significantly admixed with the O-2*p* band.

A number of theoretical calculations for bulk ZnO and its $(10\bar{1}0)$ surface have been reported [10–19]. For bulk ZnO, Mishra et al. [11] used both a scattered-wave (SW) $X\alpha$ method and an ASW (augmented spherical wave) band-structure calculation. Sukkar et al. [12] carried out a SW-$X\alpha$ calculation for a much simplified model cluster of ZnO. Pseudopotential calculations with localized Gaussian orbitals were reported by Schröer et al. [13]. LMTO (linearized muffin-tin orbital) calculations were done by Yang and Dy [14]. Xu et al. [15] employed the OLCAO (orthogonalized linear combination of atomic orbitals) method. Although most of these calculations were based on the same first principles manner, their results did not agree with each other. Schröer et al. pointed out that their theoretical density of states (DOS) for bulk ZnO did not show satisfactory agreement with the UPS experiment. They have ascribed the discrepancy to the correlation effects in the narrow *d*-band. The theoretical DOS curves of bulk ZnO by Mishra et al. and Xu et al. look similar to the result by Schröer et al., although they did not refer to the disagreement. In contrast, the Yang and Dy's

*Present address: Japan Fine Ceramics Center, 2-4-1, Mutsuno, Atsuta-ku, Nagoya, 456-8587 Japan

theoretical DOS coincides well with the UPS experiment. Recently, Vogel et al. [16] made a quantitative evaluation of the correlation effect in the narrow *d*-band, and pointed out that the discrepancy can be explained by the fault of local density approximation (LDA). They achieved good agreement between valence band structure and the experimental UPS when the LDA was corrected. However, it is still not fully persuasive for two reasons: (1) History of ZnO calculations has shown that the magnitude of the admixture of O-2*p* and Zn-3*d* is sensitive to the choice of computational method even when they were done in a ''first-principles'' manner. (2) Since UPS is very sensitive to the surface state, it is necessary to know in detail how the surface electronic structure differs from the bulk. It is still an open question whether a theoretical DOS under LDA is really unable to reproduce the experimental UPS data. The first objective of the present study is to re-examine the origin of the experimental UPS data under LDA.

The second objective of the present study is to understand the manner of interactions among atomic orbitals on the $(10\bar{1}0)$ surface of ZnO. Although the surface electronic structure has been investigated by several groups, it has not been fully understood from the viewpoint of atomic-orbital interactions. Ivanov and Pollmann [17] and Wang and Duke [18] performed empirical tight-binding calculations on the $(10\bar{1}0)$ surface of ZnO. They examined surface-induced states in detail and discussed atomic relaxation at the surface which was experimentally reported by Duke et al. [20,21] using LEED (low energy electron diffraction). Because these two results are controversial with respect to the magnitude of atomic relaxation, Schröer et al. [19] recently employed a pseudopotential technique to calculate electronic states and the magnitude of relaxation at the $(10\bar{1}0)$ surface. By total-energy minimization, they found a rotation relaxation in which both the Zn and O surface atoms move inward toward the substrate by 0.1 to 0.2Å. The relaxation, however, changes the shape of valence band structure only slightly as compared to the unrelaxed surface. Their result may be accurate and reliable with respect to the atomic relaxations. However, since they use a pseudopotential technique with Gaussian-type basis functions, interpretation of atomic interactions or bondings at the surface is not straightforward.

The method we have employed in the present work uses a numerical atomic orbital basis set that is generated by solving the radial part of the Schrödinger equation for a given chemical environment. Since the basis set produced in this way is flexible with respect to chemistry, we need a minimal number of basis functions (minimal basis set) for quantitatively reasonable computation in order to reproduce electron spectra for all sorts of compounds. A great advantage of the use of such a minimal basis set is that the atomic interactions or bondings can be intuitively interpreted. In other words, this type of computation has the virtue of yielding straightforward results for bondings.

We use the discrete variational $X\alpha$ (DV-$X\alpha$) method [22,23] throughout the present study. Tsukada et al. [24] were the first to apply this method for the computation of surface electronic structure of ZnO. Kuwabara (Sekine) et al. [25] and Sekine et al. [26] reported the DV-$X\alpha$ calculations on the polar and non-polar surfaces of ZnO. A limitation of these previous calculations is due to the insufficient consideration of electrostatic energies in the vicinity of the ZnO surfaces. Sekine et al. [25] embedded their model clusters in an external potential generated by point charges. In order to cancel the electric field gradient along the *c* axis of ZnO, they removed some point charges from the surface by a trial and error method. However, the electrostatic energy is considered to be crucial for surface electronic states of ZnO, and so it should be explicitly provided to the calculation.

Watson et al. [27] made a detailed calculation of Madelung potentials for sites in the vicinity of the ZnO surfaces using the Lennard-Jones-Dent scheme [28]. They divided a crystal into slabs parallel to the surface and evaluated lattice sums for individual slabs. In the present study, we embedded our model clusters in the external potential generated by point charges and checked for convergence by comparing the electrostatic potential with the result of Watson et al.

2. Computational Procedure

ZnO crystals have the hexagonal wurtzite structure which comprises alternating hexagonal layers of Zn atoms in a hcp lattice. O atoms are also arranged in a hcp lattice, and lie directly above each Zn atom in the direction of the *c* axis at a distance of some fraction, *u*, of the *c* axis lattice constant. According to the X-ray diffraction data by Abrahams et al. [29], *u* was

observed to be 0.3825, which is employed in the present calculation. The lattice parameters, c and a, of ZnO crystals are taken to be 5.21 and 3.25Å, respectively.

Figure 1 indicates the structures of the model clusters used in the present calculation. In the case of bulk ZnO, three types of model clusters are employed (Figs. 1(a), (b) and (c)). The smallest $(ZnO_4)^{6-}$ cluster contains a Zn atom at the center and four neighboring O atoms. This cluster is a primitive tetrahedron of the wurtzite structure. In the $(Zn_{13}O_{29})^{32-}$ cluster, a central $(ZnO_4)^{6-}$ unit is surrounded by twelve $(ZnO_4)^{6-}$ units, where the four O atoms in the central unit are shared with its neighboring units. The largest $(Zn_{57}O_{96})^{78-}$ cluster comprises the 56 neighboring tetrahedral units around the central one. These three clusters are embedded in a wurtzite-type lattice composed of ± 2 point charges, in order to take account of an electrostatic potential (Madelung potential) due to ions outside the clusters. The Madelung constant of the wurtzite structure thus obtained is confirmed to be convergent within an accuracy of 0.2% [30].

For the non-polar $(10\bar{1}0)$ surface, we employed the $(Zn_9O_{19})^{20-}$ cluster of Fig. 1(d). This cluster is obtained by removing four Zn atoms and ten O atoms along the $(10\bar{1}0)$ plane from the $(Zn_{13}O_{29})^{32-}$ cluster. In calculating the surface-model cluster, ± 2 point

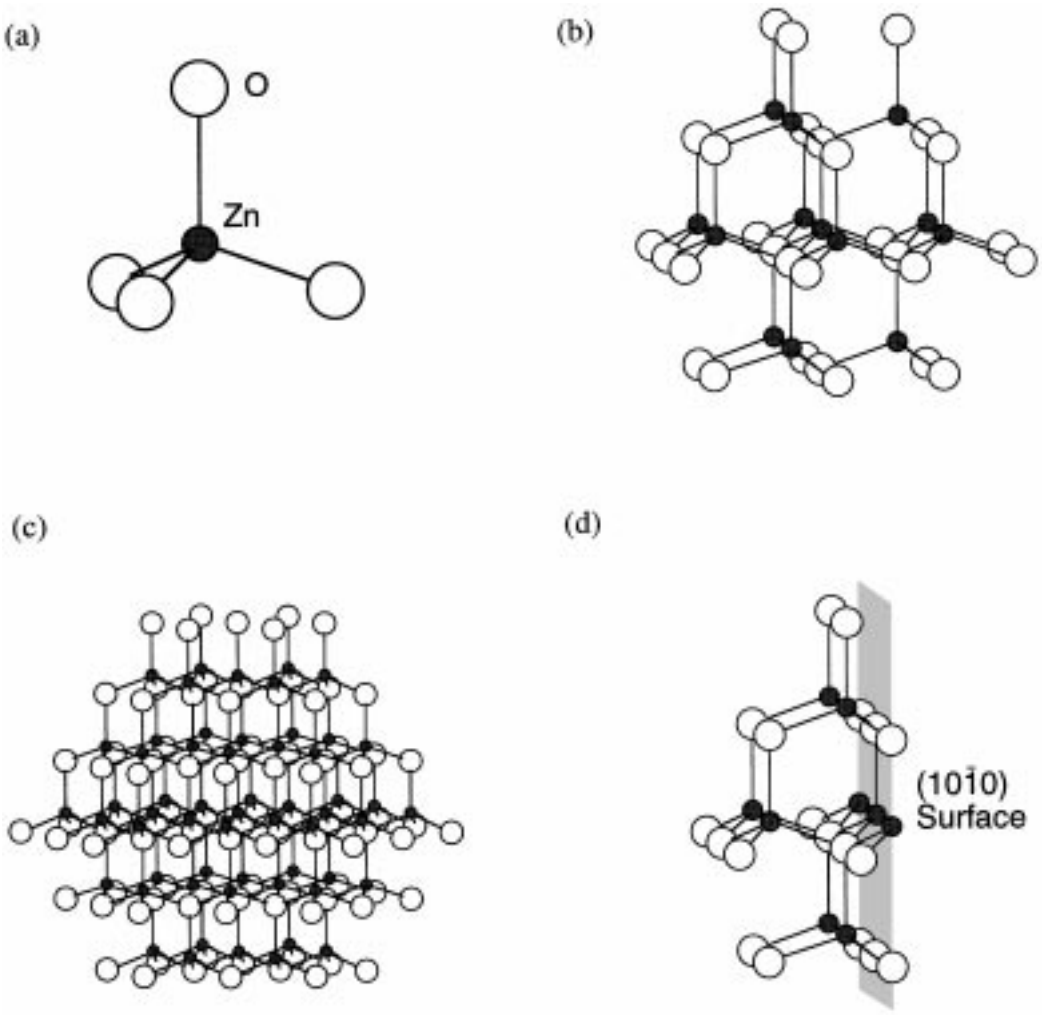

Fig. 1. Structures of model clusters used in the present study: (a) $(ZnO_4)^{6-}$, (b) $(Zn_{13}O_{29})^{32-}$, (c) $(Zn_{57}O_{96})^{78-}$ and (d) $(Zn_9O_{19})^{20-}$. Solid and open circles denote Zn and O atoms, respectively.

charges are arranged under the $(10\bar{1}0)$ surface of the cluster, so as to include an electrostatic potential near the surface. However, the electrostatic potential near the surface is considered to be different from that in bulk ZnO, due to absence of ions on one side of the lattice. Figure 2 displays the calculated electrostatic energy of an electron, V_s, at O^{2-} sites near the $(10\bar{1}0)$ surface. At Zn^{2+} sites, the magnitude of V_s is equal to that at O^{2-} sites, but the sign is positive. Note that the value of V_s on the surface layer (21.2 eV) is smaller in

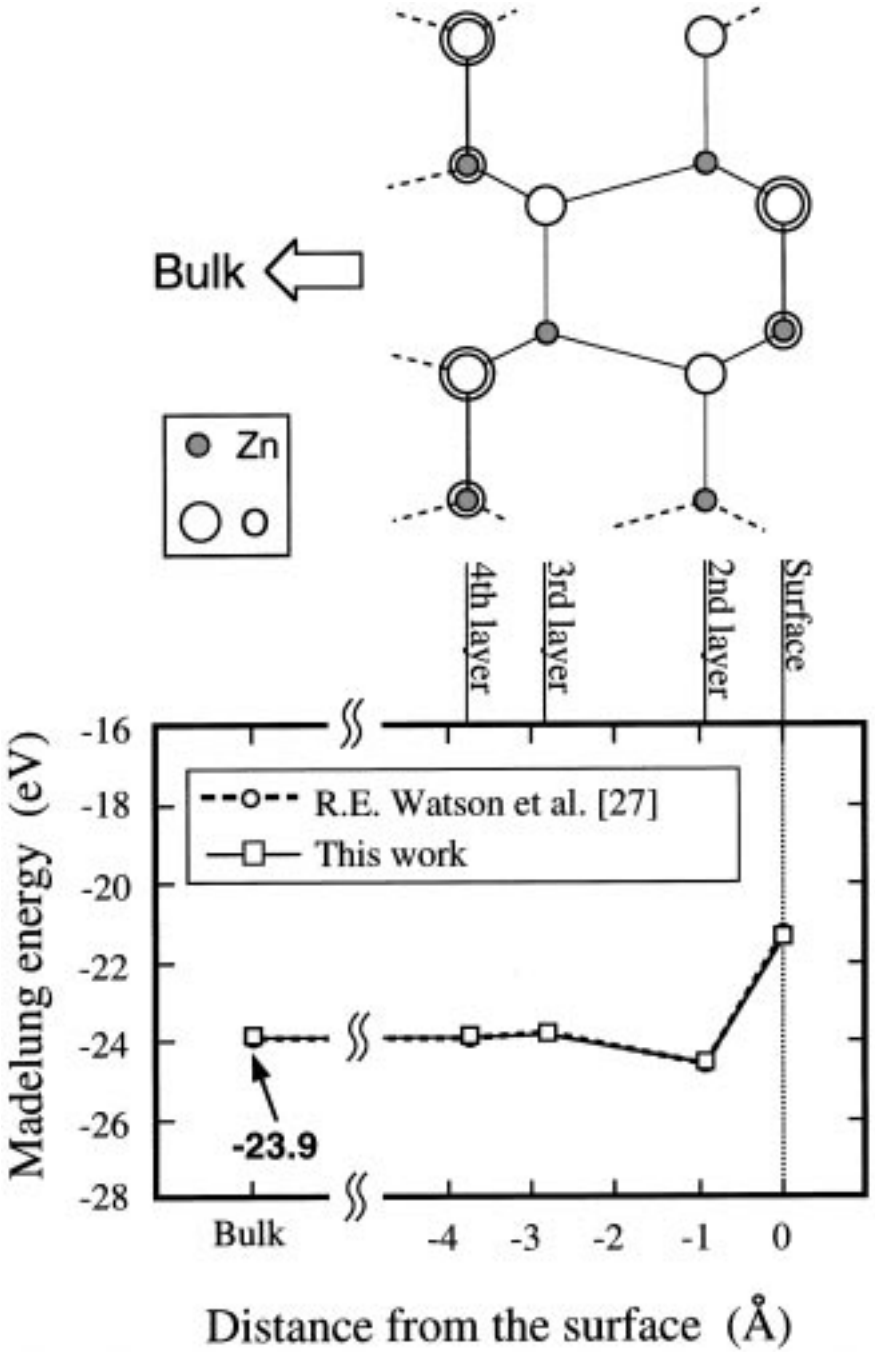

Fig. 2. Change of an electrostatic potential near the ZnO $(10\bar{1}0)$ surface.

magnitude by 2.7 eV than the bulk value (23.9 eV). As one moves away from the surface into the bulk, values of V_s first oscillate slightly and then rapidly converge to the bulk value. Below the third layer, the energy difference from the bulk value is within 0.1 eV. Such change of V_s agrees well with the results obtained by Watson et al. [27]. The $(Zn_9O_{19})^{20-}$ cluster used is embedded in such an electrostatic potential, and its electron density is calculated.

LEED studies by Duke et al. [19,20] showed that the ZnO $(10\bar{1}0)$ surface is not reconstructed, although Zn and O atoms on the surface are somewhat displaced. However, such displacements of atoms on the surface are not included in the present calculations. Since the objective of this study is to indicate a difference of valence band structures between bulk ZnO and the $(10\bar{1}0)$ surface, the general character of the valence states on the ZnO surface can be represented by calculations that exclude the surface relaxation. According to the theoretical calculation on the ZnO $(10\bar{1}0)$ surface by Schröer et al. [21], the valence band structure of the ZnO surface is not essentially affected by the surface relaxation.

First-principles calculations have been carried out using the discrete variational (DV)-$X\alpha$ method [22,23]. The electronic states of model clusters are self-consistently obtained by solving the one-electron Schrödinger equation. Molecular orbitals (MOs) thus obtained are represented by the linear combination of atomic orbitals (LCAO), as follows,

$$\phi_l(r_k) = \sum_i C_{il}\chi_i(r_k) \tag{1}$$

where $\chi_i(r_k)$ indicates atomic orbitals and r_k is one of the sampling points in the calculations. As basis sets, we employ $1s-4d$ atomic orbitals for Zn and $1s-2p$ for O, which are numerically calculated by solving the atomic Hartree-Fock-Slater equation so as to be optimized for the given chemical environment.

In order to investigate chemical bonding states of model clusters, we employ Mulliken population analysis [31]. Then, the orbital population, Q_j^l, and the overlap population, Q_{ij}^l, is given by,

$$\begin{aligned} Q_{ij}^l &= f_l C_{il} C_{jl} \sum_k \omega(r_k)\chi_i(r_k)\chi_j(r_k) \\ Q_i^l &= \sum_j Q_{ij}^l \end{aligned} \tag{2}$$

In Eq. (2), $\omega(r_k)$ is the weight of the sampling point at r_k, and f_l is the number of electrons at the l-th MO level. The sum of Q_j^l with respect to an atom A becomes an effective electron charge of the atom A. Then a net charge of the atom A is given as,

$$n_{\mathrm{A}} = Z_{\mathrm{A}} - \sum_l \sum_i Q_i^l \quad i \in \mathrm{A} \tag{3}$$

where Z_{A} is the atomic number. The sum of Q_{ij}^l between two atoms, A and B, over occupied MO levels provides a bond overlap population, $N_{\mathrm{A-B}}$,

$$N_{\mathrm{A-B}} = \sum_l \sum_{i,j} Q_{ij}^l \quad i \in \mathrm{A},\ j \in \mathrm{B} \tag{4}$$

By means of n_{A} and $N_{\mathrm{A-B}}$, the strength of ionicity and covalency can be quantified.

3. Results and Discussion

3.1. Valence Atomic Levels in ZnO

We first investigate valence atomic levels of Zn^{2+} and O^{2-} in the bulk and at the $(10\bar{1}0)$ surface. In this case, isolated Zn^{2+} and O^{2-} ions are put into an electrostatic potential generated by ± 2 point charges, as stated in section 2. ZnO is not considered to be a perfect ionic crystal, but instead is more or less covalent. However, a simple ionic model can be used to interpret the primary valence band (VB) structure of ZnO.

Figure 3 displays atomic level diagrams of Zn^{2+} and O^{2-} ions in bulk ZnO and on the $(10\bar{1}0)$ surface. When Zn^{2+} and O^{2-} ions are present in the bulk (Fig. 3(a)), the Zn-3d level is located close in energy to the O-2p level. The energy difference between the two levels is only 1.6eV. On the other hand, in the case of the $(10\bar{1}0)$ surface (Fig. 3(b)), the Zn-3d level is situated 6.9eV lower than the O-2p level. The energy difference between the two levels at the surface is much larger than in the bulk. This is due to the difference of electrostatic potentials between in the bulk and on the surface, as shown in Fig. 2. This variation of energy differences between the Zn-3d and O-2p levels will result in a difference between the VB structures of ZnO bulk and surface, although orbital interactions between Zn and O ions have not been considered in this section. Detailed VB structures of ZnO bulk and surface obtained by calculations on model clusters will be discussed in the following sections.

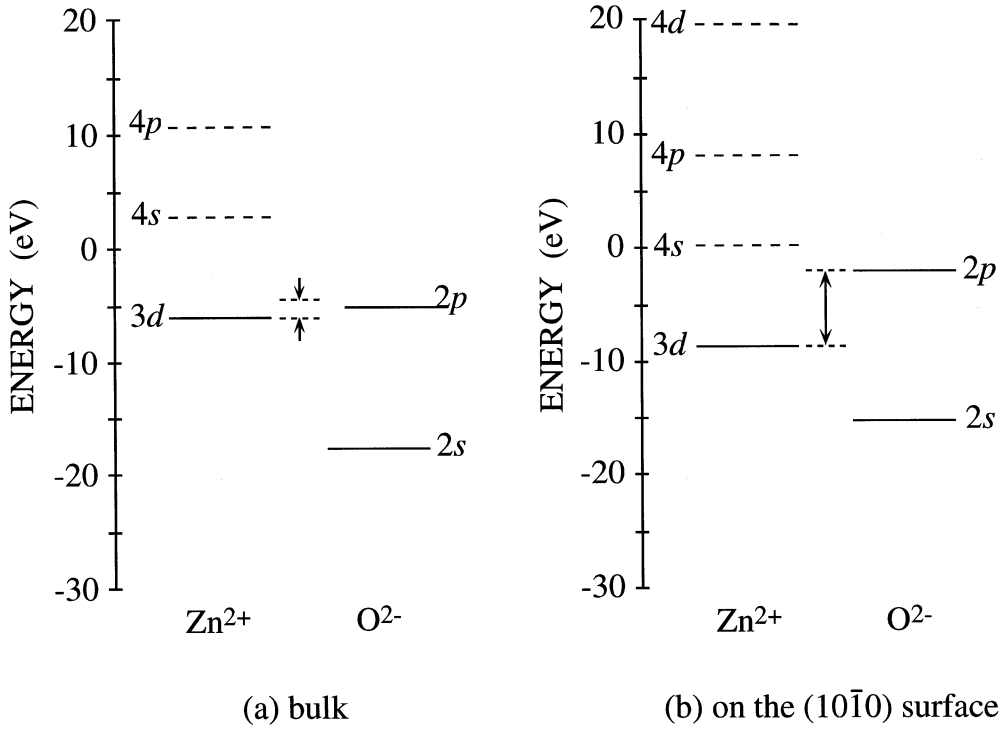

Fig. 3. Atomic level diagrams of Zn^{2+} and O^{2-} ions in electrostatic potentials generated by point charges for (a) the bulk and (b) on the $(10\bar{1}0)$ surface. Solid and broken lines denote occupied and unoccupied atomic levels, respectively.

3.2. Valence Band Structure of Bulk ZnO

MO levels calculated for bulk model clusters are shown in Fig. 4 ; (a) $(ZnO_4)^{6-}$, (b) $(Zn_{13}O_{29})^{32-}$ and (c) $(Zn_{57}O_{96})^{78-}$. HOMOs (highest occupied molecular orbitals) of these level diagrams are aligned at zero MO energy.

The upper VB of ZnO is mainly constructed by Zn-3*d* and O-2*p* orbitals, while the lower VB, which is located about 10 eV lower than the upper VB, is essentially composed of O-2*s* orbitals. Unoccupied levels mainly consist of Zn-4*s* and -4*p* orbitals, which correspond to the conduction band.

With rising cluster size, energy differences between HOMO and LUMO (lowest unoccupied molecular orbital), E_g, are seen to decrease. The value of E_g in the largest $(Zn_{57}O_{96})^{78-}$ cluster is 47% smaller than that in the smallest one. The value of E_g in the largest cluster approaches the experimental value of 3.3 eV [32]. Figure 5 shows the change of width of each band associated with increasing cluster size. Compared to the increase of the upper and lower (O-2*s*) VB widths, the unoccupied band composed of Zn-4*s* and -4*p* orbitals widens more extensively. This means that Zn-4*sp* orbitals have a large spatial distribution. Zn-4*sp* orbitals are overlapping out to the 3rd nearest neighbor Zn sites. As a result, the value of E_g becomes smaller with rising cluster size.

Next, the upper VB structure of bulk ZnO is investigated. The calculated DOS (density of states) of the $(Zn_{13}O_{29})^{32-}$ cluster is shown in Fig. 6. The DOS curve is obtained by broadening discrete MO levels by Lorentzian functions of 1.0 eV FWHM. It can be seen that the Zn-3*d* band is well admixed with the O-2*p* band in the upper VB. As stated in section 3.1, the Zn-3*d* level is located close to the O-2*p* level in bulk ZnO, so that the Zn-3*d* band strongly interacts with the O-2*p* band. Zn-4*s* and -4*p* components also contribute slightly to the upper VB. The upper VB structure of the $(Zn_{13}O_{29})^{32-}$ cluster is the same as that of the largest $(Zn_{57}O_{96})^{78-}$ cluster, which is not shown here. The profile of the obtained DOS curve are in good agreement with the first-principles theoretical calculation on bulk ZnO by Xu et al. [15].

As shown above, the VB of bulk ZnO exhibits the strong admixture of Zn-3*d* and O-2*p* orbitals. In the

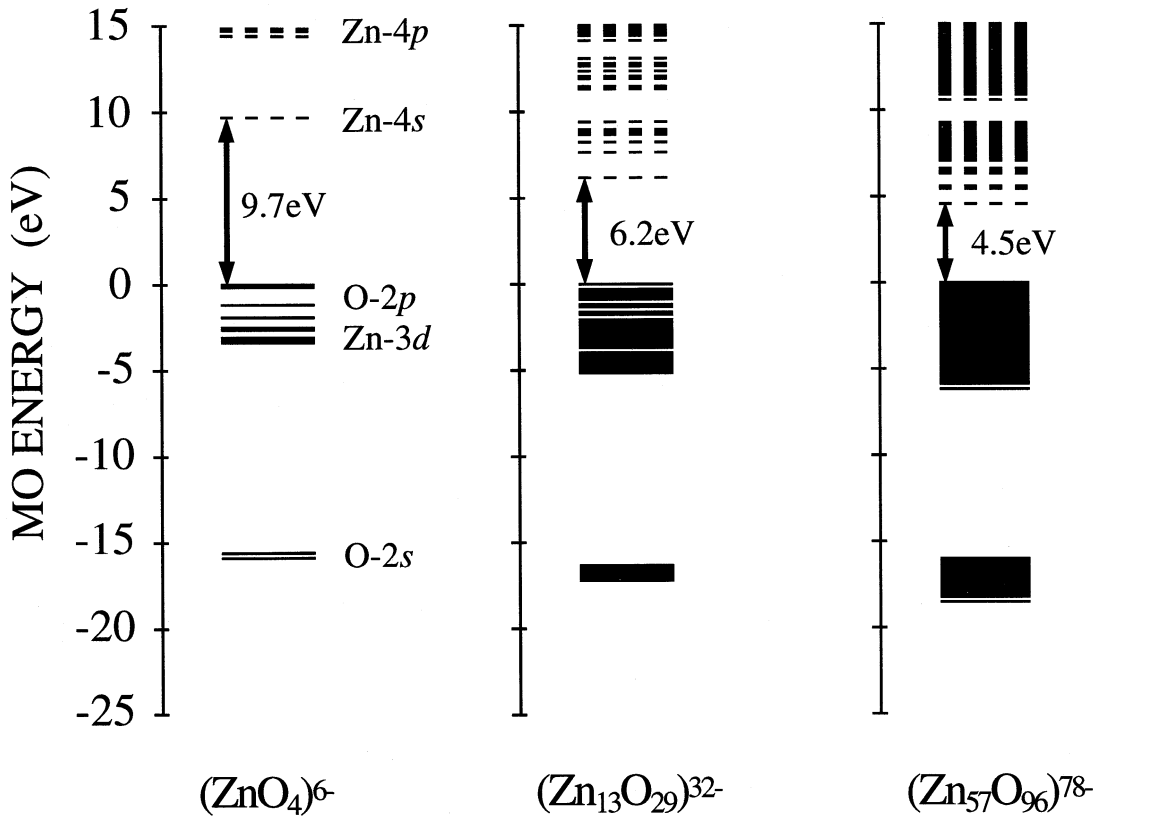

Fig. 4. MO level diagrams for bulk model clusters: (a) $(ZnO_4)^{6-}$, (b) $(Zn_{13}O_{29})^{32-}$, (c) $(Zn_{57}O_{96})^{78-}$. Solid and broken lines denote occupied and unoccupied MO levels, respectively.

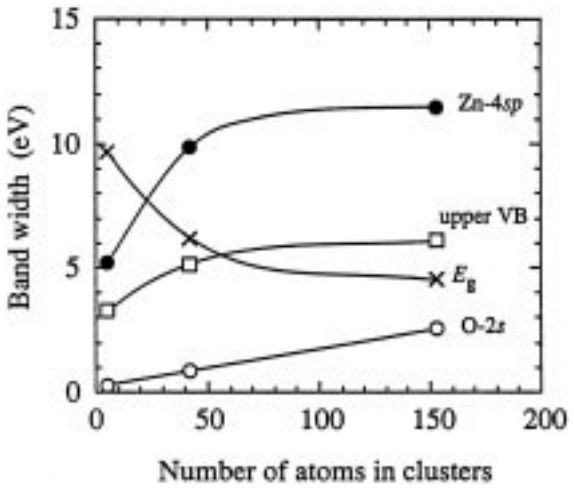

Fig. 5. Change of each band width for the bulk clusters as a function of the number of atoms in the clusters.

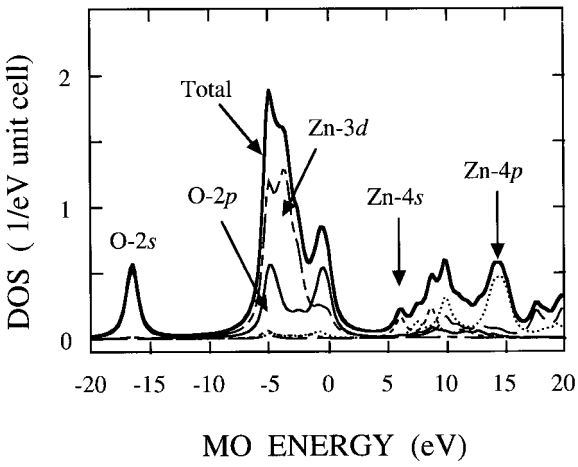

Fig. 6. The DOS (density of states) in the valence band for the $(Zn_{13}O_{29})^{32-}$ cluster.

next section, the VB structure at the $(10\bar{1}0)$ surface will be shown, in comparison with the bulk VB structure.

3.3. Valence Band of ZnO $(10\bar{1}0)$ *Surface*

In the case of the ZnO surface, a change of electronic structures is examined. Figure 7 displays a MO level diagram calculated for the $(Zn_9O_{19})^{20-}$ cluster. For comparison, the result on the $(Zn_{13}O_{29})^{32-}$ cluster (bulk model) is shown. As can be seen in this figure, the upper and lower VB widths become broader than those in the bulk cluster. The energy difference between HOMO and LUMO in the surface cluster is 3.1 eV. The LUMO is mainly composed of 4*s* orbitals of Zn at the $(10\bar{1}0)$ surface, so that this can be referred to as a surface-induced level. As compared to the intrinsic band gap experimentally reported (3.3 eV [32]), the surface level can be considered to be located near the conduction-band edge of ZnO.

In order to investigate the VB structure of the surface-model cluster, the DOS curve is depicted in

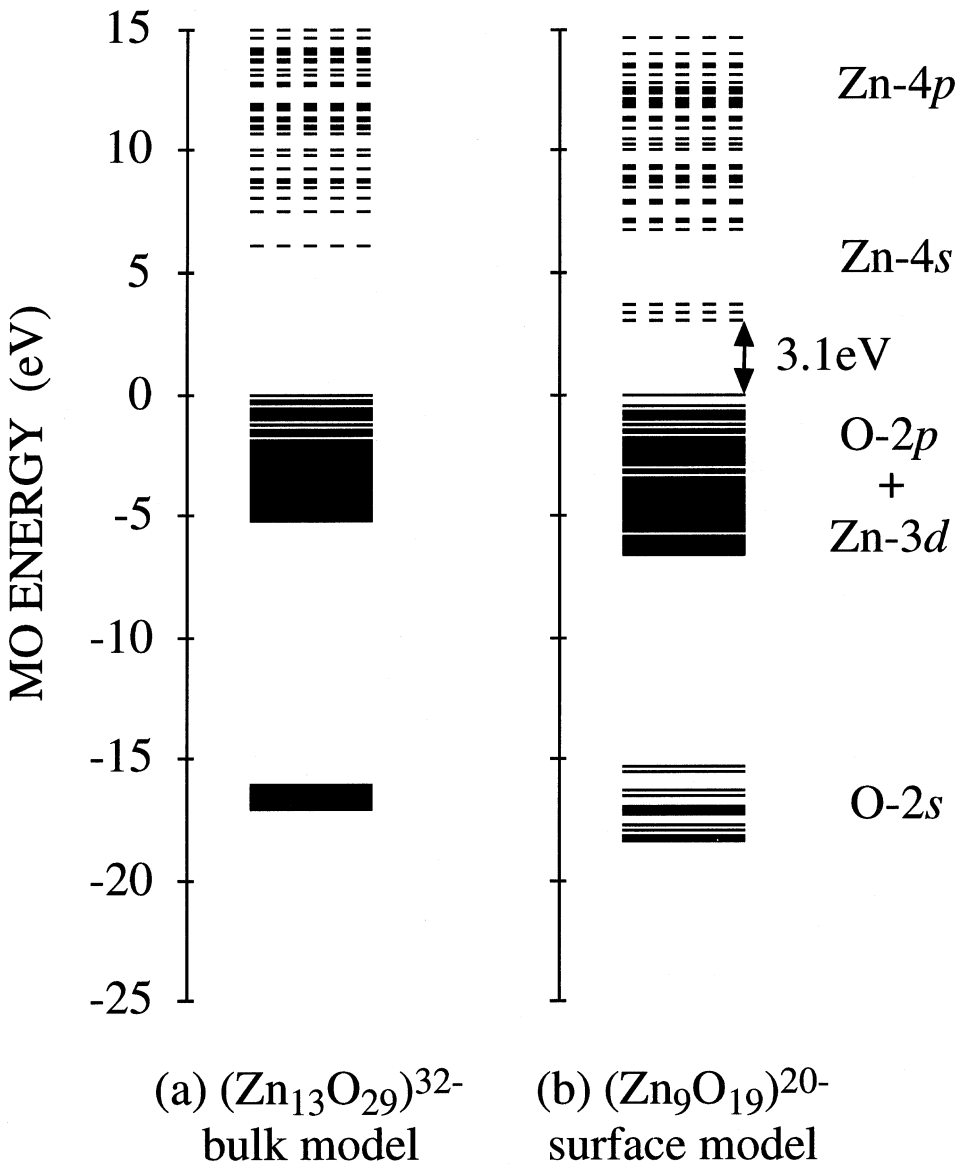

Fig. 7. MO level diagrams for (a) the bulk-model and (b) the surface-model clusters.

Fig. 8(a), similar to Fig. 6. We make a comparison with the experimental UPS spectrum at the $(10\bar{1}0)$ surface of ZnO [5]. The DOS curve is the local DOS of Zn and O at the $(10\bar{1}0)$ surface extracted from the total DOS of the cluster.

The upper VB of the $(10\bar{1}0)$ surface is also seen to be composed of Zn-3*d* and O-2*p* bands. Note that the Zn-3*d* band has little admixture with O-2*p* orbitals. This is a striking contrast with the bulk DOS (Fig. 6), where the Zn-3*d* band strongly interacts with the O-2*p* band. Such a difference of the VB structure can be explained in terms of the difference of electrostatic potentials between the bulk and the surface. As shown in Figs. 3(a) and (b), the energy difference between Zn-3*d* and O-2*p* levels on the surface is larger than that in the bulk. Thus the admixture between the Zn-3*d* and O-2*p* bands on the surface is not so strong as that in the bulk. The profile of the DOS curve for the surface cluster is found to be in good agreement with the experimental spectrum. Although the largest peak in the lower part of the upper VB, which is mainly composed of Zn-3*d* orbitals, is located about 2.0 eV higher than that in the experiment, the general features of the UPS spectrum can be well reproduced by the present calculation.

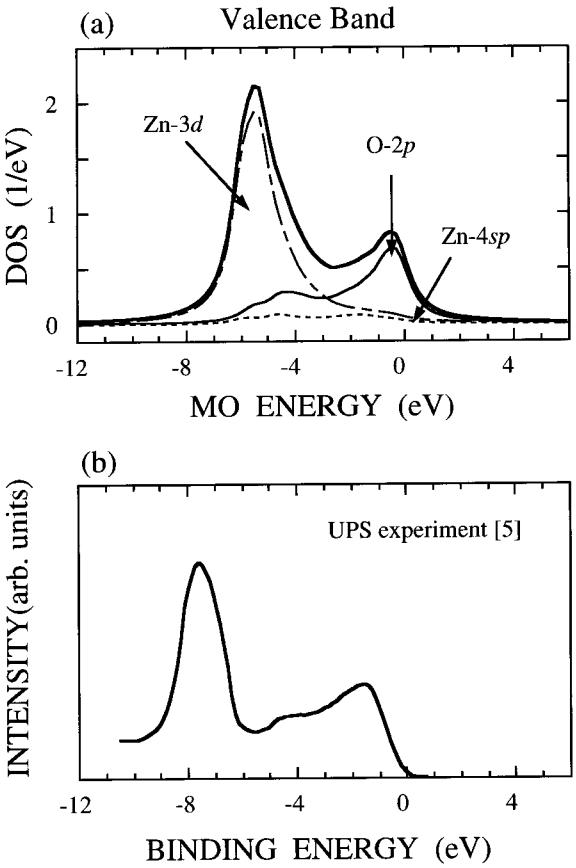

Fig. 8. The DOS in the upper valence band on the ZnO $(10\bar{1}0)$ surface calculated for the $(Zn_9O_{19})^{20-}$ cluster (a). The lower figure is the experimental UPS spectrum obtained by Göpel et al. [5].

As discussed above, the DOS curve at the ZnO $(10\bar{1}0)$ surface is found to differ from that in the bulk. This fact is significant for analysis of the experimental spectrum on the ZnO surface, and may change the chemical bonding states in ZnO. The chemical bonds of ZnO are considered in the next section.

3.4. Chemical Bonding of ZnO Surface

Mulliken population analysis was used to compare chemical bonds for the $(Zn_{13}O_{29})^{32-}$ and $(Zn_9O_{19})^{20-}$ clusters. Net charges of Zn and O in the $(Zn_{13}O_{29})^{32-}$ and $(Zn_9O_{19})^{20-}$ clusters are shown in Table 1. In the case of the $(Zn_9O_{19})^{20-}$ cluster (surface model), net charges of atoms at the surface are listed. The calculated values of n_{Zn} and n_O in bulk ZnO are found to be about a half of their formal charges, ± 2, while Zn and O atoms on the $(10\bar{1}0)$ surface exhibit slightly smaller net charges than those in the bulk. Thus, in ZnO, the Zn-O bond is predicted to substantially covalent. Thus overlap populations between Zn and O in the upper VB are examined.

Figure 9 shows diagrams of overlap populations between Zn and O in the upper VB. In the case of the surface model (b), overlap populations of Zn-O at the surface are displayed. In the bulk ZnO (a), the Zn-3*d* band has bonding interactions with the O-2*p* band in the lower part of the VB. In addition, anti-bonding interactions of Zn-O can also be seen in the upper part of the VB. The strong admixture of Zn-3*d* and O-2*p* bands in bulk ZnO results in these strong bonding and anti-bonding interactions. However, the net overlap population between Zn-3*d* and O-2*p* orbitals, which is a sum of the bonding and anti-bonding contributions between the two orbitals, is almost zero (-0.03). On

Table 1. Net charges of Zn and O in the bulk-model and surface-model clusters

	Zn	O
$(Zn_{13}O_{29})^{32-}$ bulk	+1.03	−1.04
$(Zn_9O_{19})^{20-}$ surface	+0.97	−1.03

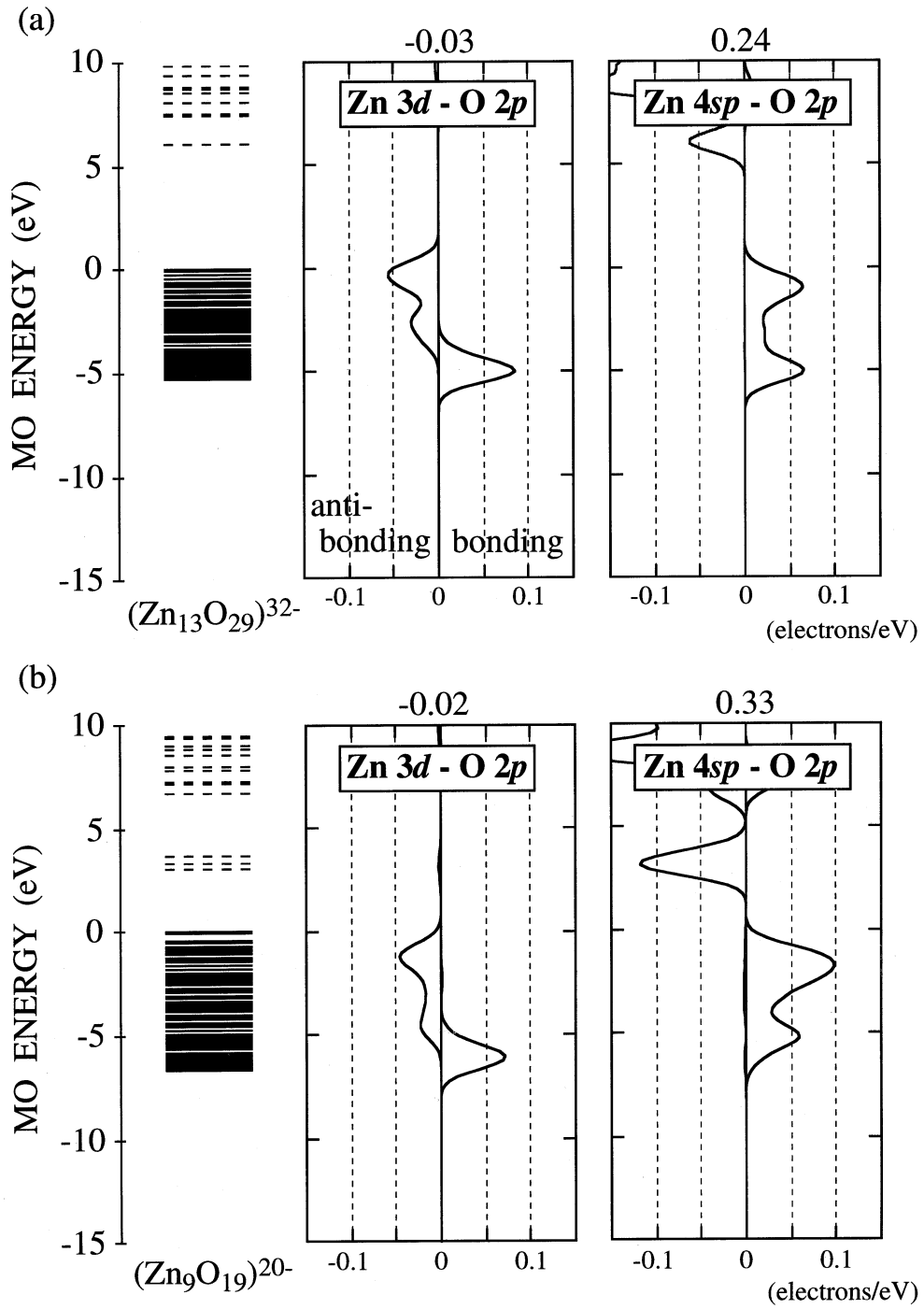

Fig. 9. Diagrams of overlap populations in (a) the $(Zn_{13}O_{29})^{32-}$ and (b) the $(Zn_9O_{19})^{20-}$ clusters. The right side of each diagram denotes bonding overlap between two orbitals, and the left side anti-bonding. Net overlap populations between two orbitals are shown at the top of each diagram.

the other hand, it can be seen in Fig. 9(b) that the overlap between the Zn-3*d* and O-2*p* bands at the $(10\bar{1}0)$ surface is slightly smaller than that in the bulk. The energy separation between Zn-3*d* and O-2*p* levels due to the effect of electrostatic potentials at the surface (see Fig. 3(b)) leads to less overlap of the two bands in the upper VB. However, in this case, the net overlap population of Zn-3*d* and O-2*p* orbitals is also almost zero (-0.02). Therefore, the interactions between Zn-3*d* and O-2*p* orbitals do not actually contribute to covalent bonds of Zn-O.

Zn-4*s* and -4*p* components also contribute to the upper VB. As can be seen in Fig. 9, Zn-4*sp* orbitals have bonding interactions with O-2*p* orbitals in the upper VB, leading to covalent bonds of Zn-O. Such bonding interactions of Zn-4*sp* and O-2*p* orbitals in the case of the $(10\bar{1}0)$ surface (b) are much larger than those in the bulk. This can also be interpreted by considering the simple ionic model shown in Fig. 3. As compared to the case of bulk ZnO, the energy separation between Zn-3*d* and O-2*p* levels on the surface is much larger. At the same time, the Zn-4*s* and -4*p* levels on the surface are situated closer to the O-2*p* level. This results in the stronger bonding overlap of Zn-4*sp* and O-2*p* orbitals in the upper VB of the surface. Thus, the net overlap population of Zn-4*sp* and O-2*p* on the surface is larger than that in the bulk.

A total sum of overlap populations over occupied levels between Zn and O gives rise to a bond overlap population of Zn-O. Table 2 gives values of bond overlap populations of Zn-O. The $N_{\text{Zn-O}}$ on the surface is found to be 48% larger than the $N_{\text{Zn-O}}$ in the bulk. This is mainly due to the stronger bonding interactions of Zn-4*sp* and O-2*p* orbitals. Therefore, a Zn-O bond on the surface has stronger covalency than one in the bulk.

4. Conclusions

We have performed first-principles molecular orbital calculations on the bulk and the surface valence band structures of ZnO, using the DV-Xα cluster method. The results obtained are summarized as follows.

1. The valence band of ZnO, which is formed by Zn-3*d* and O-2*p* orbitals, is found to be greatly influenced by the electrostatic potentials in the bulk and at the surface. In the case of the bulk ZnO, the Zn-3*d* and O-2*p* orbitals are strongly admixed in the valence band. The valence band at the surface, however, exhibits less admixture between the two orbitals. The changes in the valence band between the bulk and the surface are caused by the reduction of the electrostatic potentials near the surface, compared to the bulk. The calculated DOS in the valence band of the surface showed a good agreement with the experimental UPS spectrum. Therefore, the origin of the experimental UPS spectrum can be interpreted by considering the change of the electrostatic potentials at the surface.

2. In consequence of the surface electronic structure of ZnO, the chemical bonding of ZnO at the surface is also different from that in the bulk. The Zn-O covalent bond at the non-polar surface is found to be much stronger than that in the bulk. Although ZnO is sometimes considered to be an ionic compound, the covalency on the ZnO surface is not negligible. The above result would be important in relation to chemical reactions in catalytic processes at the surface.

ZnO is an important material on its peculiar phenomena in regions of surfaces and grain boundaries. For the purpose of detailed analyzes on such phenomena, the characteristic electronic structure of ZnO should be clarified from first-principles calculations. Our present results will be useful not only for the interpretation of the electronic structure on the ZnO surface, but also for future studies on more realistic systems involving defects, impurities, interfaces and adsorbed atoms. The characteristic chemical bonding state on the surface (more covalent than in the bulk) should be significant in considering a chemical reaction at ZnO surfaces with adsorbed molecules or atoms in detail.

Table 2. Bond overlap populations of Zn-O in the bulk-model and surface-model clusters

	Zn-O
$(Zn_{13}O_{29})^{32-}$ bulk	0.25
$(Zn_9O_{19})^{20-}$ surface	0.37

Acknowledgment

This study was performed through Special Coordination Funds of the Science and Technology Agency of the Japanese Government.

References

1. V. E. Henrich and P. A. Cox, *The Surface Science of Metal Oxides* (Cambridge, New York, 1994).
2. Y. M. Chiang, D. P. Birnie, and W. D. Kingery, *Physical Ceramics* (John Wiley & Son, New York, 1997).
3. H. Lüth, G. W. Rubloff, and W. D. Grobman, *Solid State Commun.*, **18**, 1427 (1976).
4. W. Göpel, R. S. Bauer, and G. Hausson, *Surf. Sci.*, **99**, 138 (1980).
5. W. Göpel, J. Pollmann, I. Ivanov, and B. Reihl, *Phys. Rev.*, **B26**, 3144 (1982).
6. W. Ranke, *Solid State Commun.*, **19**, 685 (1976).
7. S. V. Didziulis, S. L. Cohen, K. D. Butcher, and E. I. Solomon, *Inorg. Chem.*, **27**, 2238 (1988).
8. K. Jacobi, G. Zwicker, and A. Gutmann, *Surf. Sci.*, **141**, 109 (1984).
9. L. Ley, R. A. Pollak, F. R. McFeely, S. P. Kowalczyk, and D. A. Shirley, *Phys. Rev.*, **B9**, 600 (1974).
10. S. Bloom and I. Ortenburger, *Phys. Stat. Sol.*, (b) **58**, 561 (1973).
11. K. C. Mishra, P. C. Schmidt, K. H. Johnson, B. G. DeBoer, J. K. Berkowitz, and E. A. Dale, *Phys. Rev.*, **B42**, 1423 (1990).
12. M. H. Sukkar, K. H. Johnson, and H. L. Tuller, *Mater. Sci. Eng.*, **B6**, 49 (1990).
13. P. Schröer, P. Krüger, and J. Pollmann, *Phys. Rev.*, **B47**, 6971 (1993).
14. C. K. Yang and K. S. Dy, *Solid State Commun.*, **88**, 491 (1993).
15. Y. N. Xu and W. Y. Ching, *Phys. Rev.*, **B48**, 4335 (1993).
16. D. Vogel, P. Krüger and J. Pollmann, *Phys. Rev.*, **B54**, 5495 (1996).
17. I. Ivanov and J. Pollmann, *Phys. Rev.*, **B24**, 7275 (1981).
18. Y. R. Wang and C. B. Duke, *Surf. Sci.*, **192**, 309 (1987).
19. P. Schröer, P. Krüger, and J. Pollmann, *Phys. Rev.*, **B49**, 17092 (1994).
20. C. B. Duke, A. R. Lubinsky, S. C. Chang, B. W. Lee, and P. Mark, *Phys. Rev.*, **B15**, 4865 (1977).
21. C. B. Duke, R. J. Meyer, A. Paton, and P. Mark, *Phys. Rev.*, **B18**, 4225 (1978).
22. D. E. Ellis, H. Adachi, and F. W. Averill, *Surf. Sci.*, **58**, 497 (1976).
23. H. Adachi, M. Tsukada, and C. Satoko, *J. Phys. Soc. Jpn.*, **45**, 875 (1978).
24. M. Tsukada, E. Miyazaki, and H. Adachi, *J. Phys. Soc. Jpn.*, **50**, 3032 (1981).
25. R. Kuwabara, H. Adachi, and T. Morimoto, *Surf. Sci.*, **193**, 271 (1988).
26. R. Sekine, H. Adachi, and T. Morimoto, *Surf. Sci.*, **208**, 177 (1989).
27. R. E. Watson, M. L. Perlman, and J. W. Davenport, *Surf. Sci.*, **115**, 117 (1982).
28. J. E. Lennard-Jones and B. M. Dent, *Trans. Faraday Soc.*, **24**, 92 (1928).
29. S. C. Abrahams and J. L. Bernstein, *Acta Cryst.*, **B25**, 2254 (1969).
30. H. Coker, *J. Phys. Chem.*, **87**, 2512 (1983).
31. R. S. Mulliken, *J. Chem. Phys.*, **23**, 1833 (1955).
32. *Handbook of Laser Science and Technology*, edited by M. J. Weber (CRC, Cleveland, 1986), Vol. III.